ROYAL SOCIETY OF CHEMISTRY

www.rsc.org/pccp

Journal Name

ARTICLE

Rotational spectroscopy of methyl benzoylformate and methyl mandelate: structure and internal dynamics of a model reactant and product of enantioselective reduction

Received 00th January 20xx,
Accepted 00th January 20xx

DOI: 10.1039/x0xx00000x

www.rsc.org/

Elijah G. Schnitzler, Mohammad Reza Poopari, Yunjie Xu and Wolfgang Jäger

Pure rotational spectra of a prototypical prochiral ester, methyl benzoylformate (MBF), and the product of its enantioselective reduction, (R)-(–)-methyl mandelate (MM), were measured in the range of 5-16 GHz, using a cavity-based molecular beam Fourier-transform microwave spectrometer. Potential conformers were located using density functional theory calculations, and one conformer of each species was identified experimentally. The minimum energy conformer of MBF, in which the ester group is in a *Z* orientation, was observed for the first time. Based on an atoms-in-molecules analysis, MBF contains a weak CH···O=C hydrogen bond between the carbonyl oxygen atom of the ester group and the nearest hydrogen atom of the aromatic ring. In the minimum energy conformer of MM, the ester group is oriented to accommodate a hydrogen bond between the hydrogen atom of the hydroxyl group and the carbonyl oxygen atom (OH···O=C), rather than the sp^3 oxygen atom (OH···O–C). For both species, splittings of the rotational transitions were observed, which are attributed to methyl internal rotation, and the orientations and barrier heights of the methyl tops were determined precisely. The barrier heights for MBF and MM are 4.60(2) and 4.54(3) kJ mol^{-1}, respectively, which are consistent with values predicted by high-level wavefunction-based calculations. On the basis of an atoms-in-molecules analysis, we propose that destabilization of the sp^3 oxygen atom of the ester group most directly dictates the barrier height.

Introduction

In organisms, metabolism of biomolecules is carried out by enantioselective enzymes and coenzymes.[1] For example, in its reduced form, the coenzyme nicotinamide adenine dinucleotide (NADH) facilitates enantioselective reduction of many biomolecules.[2] Over the years, numerous NADH mimics have been synthesized by organic chemists for use as enantioselective reducing agents in the laboratory.[3-5] Many of these mimics were designed and/or evaluated for the reduction of prochiral benzoylformates, resulting in optically pure *R*- or *S*-mandelates;[6] in particular, reduction of methyl benzoylformate (MBF) resulting in methyl mandelate (MM) is by far the most commonly investigated reaction.[7-13] Recently, this reaction was also used to characterize more unconventional enantioselective catalysts, including heterogeneous platinum-supported[14] and nano-confined[15] catalysts. Consequently, the pair of MBF and MM is an excellent model system of a reactant and product of enantioselective reduction, in general.

Despite its significance as a model reactant, MBF has not been characterized using spectroscopic methods in the past. In contrast, due to its more general role as a model chiral species, MM has been studied extensively. In a relatively early study, Suryanarayana et al. observed that the frequency of the OH stretching vibration of MM in solution increases as solvents that increasingly disrupt the intramolecular hydrogen bonding of MM are used.[16] More recently, based on resolved OH stretching vibrational bands of MM in *n*-hexane, Tsui et al. distinguished two intramolecular hydrogen bonding scenarios: OH hydrogen-bonded to the sp^3-hybridized oxygen atom of the ester group (OH···O–C); and OH hydrogen-bonded to the sp^2-hybridized oxygen atom of the carbonyl group (OH···O=C).[17] Le Barbu-Debus et al. assigned their double-resonance IR/UV spectrum of MM in the gas phase to the latter conformer, containing an OH···O=C intramolecular hydrogen bond, which they also calculated to be the minimum energy conformer.[18] Albrecht et al. followed up on this study by investigating self-aggregation of MM, using a wide variety of spectroscopic methods.[19] Furthermore, Nedić and Suhm characterized crystalline MM using Fourier-transform infrared microspectroscopy,[20] and Poopari et al. characterized solvated MM using vibrational circular dichroism.[21] Finally, Shi et al. used MM as a representative species in their computational model of chirality recognition.[22]

Rotational spectroscopy is a powerful method for determining the structure of molecules in the gas phase. For example, the simplest ester, methyl formate, has been studied

---

Department of Chemistry, University of Alberta, 11227 Saskatchewan Drive, Edmonton, Alberta T6G 2G2, Canada.

†Electronic Supplementary Information (ESI) available: Tables of rotational transition frequencies and molecular graphs of atoms-in-molecules analysis. See DOI: 10.1039/x0xx00000x

extensively using rotational spectroscopy,[23-25] which also led to its detection in the interstellar medium.[26,27] Furthermore, several larger, more complicated esters have also been investigated, including methyl salicylate,[28] methyl lactate,[29,30] and methyl glycidate;[31] the latter two, like MM, are also model chiral species. The rotational spectra of all of the above esters exhibit splittings due to internal rotation of the methyl top of the ester group. The internal dynamics and, more specifically, the heights of the three-fold barriers to rotation were probed precisely.

Here, we present pure rotational spectra of MBF and MM, measured in the range of 5-16 GHz using a cavity-based molecular beam Fourier-transform microwave (MB-FTMW) spectrometer. Conformers were located using density functional theory (DFT) calculations; one conformer of each species is assigned to the observed spectra. The geometry of the minimum energy conformer of MBF has been determined for the first time; it has the methyl and carbonyl moieties of the ester group in a syn orientation to each other. The minimum energy conformer of MM is the same one identified earlier, based on other spectroscopic methods; it contains an intramolecular hydrogen bond (OH···O=C), which we characterize using the quantum theory of atoms-in-molecules (QTAIM). Based on a QTAIM analysis of MBF, a weak hydrogen bond forms between the carbonyl oxygen atom of the ester group and the nearest hydrogen atom of the aromatic ring (CH···O=C). In the spectra of both MBF and MM, splittings were observed, because of internal rotation of the methyl top of the ester group; consequently, we were able to determine the heights of the respective three-fold barriers to rotation, which are in good agreement with those calculated at the MP2/6-311++G(d,p) level of theory. Finally, the barriers to internal rotation are rationalized in terms of QTAIM.

Methods

Experimental

Reagent grade MBF (Aldrich, 98%) and (R)-(–)-MM (Alfa Aesar, 99%) were used without further purification. At room temperature, MBF is a liquid, and MM is a solid; however, the vapour pressures of both species are very low. Consequently, we heated samples to about 323 K in a small stainless steel chamber; directly downstream, the nozzle used to introduce the species into the spectrometer was heated to a few degrees higher than the sample container. In earlier studies, this approach was found to be effective for species of similar and even lower volatilities.[32,33] Neon was used as backing gas at pressures between 1 and 2 atm; a heated coil of copper tubing was used to pre-heat the gas stream before it reached the sample chamber.

The MB-FTMW spectrometer has been described in detail in the past.[34-36] In brief, each experiment cycle begins with the injection of sample through a pulsed nozzle into a high vacuum chamber housing two aluminum mirrors, which constitute the microwave resonator. One mirror is translated to adjust the cavity into resonance with the frequency of the applied radiation. A supersonic expansion results from the difference in pressure across the nozzle, and the sample is cooled to a rotational temperature of about 1 K, through many collisions with the backing gas. Following injection, a microwave excitation pulse is introduced to align the dipoles of the molecules, resulting in a macroscopic polarization of the molecular ensemble. After excitation, emission from the molecular ensemble at the transition frequency is detected as a free induction decay in the time domain. The signal is digitized and converted into a spectrum in the frequency domain using a Fourier-transformation. Because the molecular expansion and the resonator axis are oriented co-axially, both backward and forward (reflected) emission from the molecular ensemble is detected, so each transition is split into a Doppler pair. The average frequency of each pair is used as the corresponding rest frequency.

Computational

The minimum energy structures of MBF and MM were determined using DFT calculations, as implemented in Gaussian 09.[37] For both MBF and MM, we located conformers by systematically stepping the dihedral angle about each rotatable bond through a full revolution and optimizing the remaining internal coordinates, using the B3LYP functional[38] with the 6-311++G(d,p) Pople basis set.[39] Subsequently, minima along these scans of the potential energy surface were used as input structures in full geometry optimization and frequency analysis calculations. Minimum energy structures were verified by confirming that no imaginary frequencies occurred. The zero-point energy (*ZPE*) of each minimum was determined from its frequency analysis and added to the electronic energy to give the *ZPE*-corrected energy. Hydrogen bonding and methyl internal rotation were investigated using QTAIM,[40,41] as implemented in Multiwfn.[42] Errors in atomic energies incurred during numerical integration were corrected using the virial ratio.[43]

The calculated rotational constants of the conformers were used to generate predicted rotational spectra in PGOPHER.[44] Preliminary fits of the A symmetry components of transitions were also carried out in PGOPHER. Final fits of both A and E symmetry components were carried out using XIAM,[45] an internal rotation program, implemented using the combined axis method. Watson's A-reduction Hamiltonian was used in the spectral fits.[46]

Results and discussion

Structure

Using the above approach, two conformers of MBF were located, as illustrated in Fig. 1. In both conformers, the carbonyl group adjoining the phenyl and ester groups is in the same plane as the aromatic ring, and the ester group is rotated out of the plane, such that the O=C–CO dihedral angle is about 60°. The two conformers differ with respect to the CC(=O)–OC(H_3) dihedral angle. In the lowest energy conformer, MBF-I, the methyl group is oriented in the *Z* conformation (with a dihedral angle of about 175°); in the higher energy conformer, MBF-II, the methyl group is rotated roughly 180° to the *E* conformation. The calculated rotational constants and dipole moments are listed in Table 1.

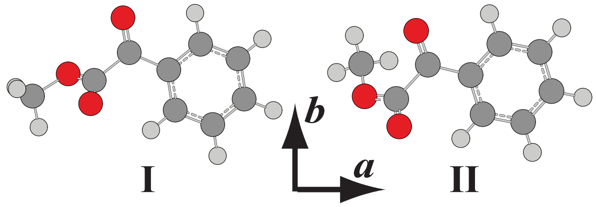

Fig. 1 Conformers of methyl benzoylformate, optimized at the B3LYP/6-311++G(d,p) level of theory.

Table 1 Calculated relative energies, abundances, rotational constants, and dipole moments of two conformers of methyl benzoylformate at the B3LYP/6-311++G(d,p) level of theory

Constant	MBF-I	MBF-II
ΔE^a/kJ mol^{-1}	0.00	21.9
ΔG^b/kJ mol^{-1}	0.00	23.4
P^c/%	>99.9	0.02
A/MHz	2199.44	1942.50
B/MHz	545.38	592.01
C/MHz	469.45	526.11
κ^d	-0.91	-0.91
$\lvert\mu_a\rvert$/D	0.94	2.72
$\lvert\mu_b\rvert$/D	2.24	0.98
$\lvert\mu_c\rvert$/D	1.70	3.51

[a] Total energy (sum of electronic and zero-point energies) relative to minimum energy conformer. [b] Relative free energy. [c] Percent abundance at 323 K, the source temperature, based on relative free energy. [d] Asymmetry parameter, $\kappa = (2B - A - C)/(A - C)$.

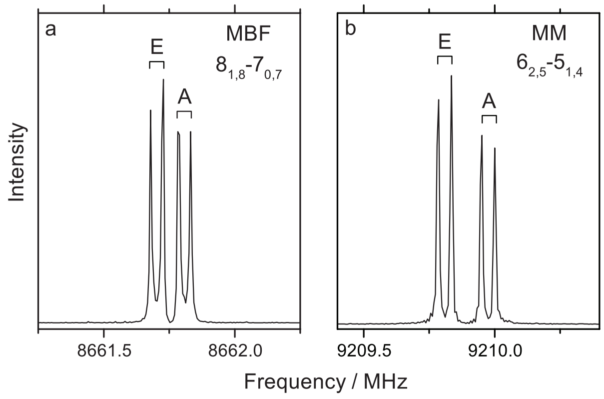

Fig. 2 Representative *b*-type transitions of (a) methyl benzoylformate and (b) methyl mandelate. Both transitions were measured using a 0.5 mW excitation pulse with a duration of 0.6 μs. Panel (a) and (b) illustrate averages of 100 and 200 cycles, respectively.

The relative *ZPE*-corrected energies and free energies are also listed in Table 1, and they are consistent with the well-known general preference of esters for the *Z* conformation.[47] At the B3LYP/6-311++G(d,p) level, MBF-II is about 23.4 kJ mol^{-1} higher in free energy than MBF-I; consequently, even at the elevated sample temperature of 323 K, the abundance of MBF-II is predicted to be very low, only 0.02%, so we targeted transitions of MBF-I during our spectral search. A representative transition, exhibiting methyl internal rotation splitting, is shown in Fig. 2. The observed lines were fitted to determine the rotational, centrifugal distortion, and internal rotation constants listed in Table 2. As shown in Table S1, 42 transitions were measured: 6 *a*-type, 22 *b*-type, and 14 *c*-type. On average, the calculated rotational constants of MBF-I are only 0.5% lower than those determined experimentally. The experimental centrifugal distortion constants – Δ_J, Δ_{JK}, Δ_K, δ_J, and δ_K – are remarkably consistent with predicted values of 0.0354, -0.4347, 4.1030, -0.0004, and -0.2601 kHz, respectively, based on a harmonic vibrational frequency calculation. Furthermore, *b*-type transitions required the shortest microwave pulse width to reach their maximum signal-to-noise ratio, consistent with the largest predicted *b*-dipole moment component, 2.2 D, of MBF-I among all three types. On these grounds, we assign the experimental spectrum to MBF-I. Our results constitute the first determination of the structure of MBF in the gas phase.

Table 2 Experimental rotational constants, centrifugal distortion constants, and internal rotation constants of methyl benzoylformate and methyl mandelate

Constant	MBF	MM
A/MHz	2211.4648(7)	1559.9360(3)
B/MHz	549.1940(1)	650.4152(2)
C/MHz	470.8890(2)	539.8728(1)
Δ_J/kHz	0.0425(9)	0.094(1)
Δ_{JK}/kHz	-0.564(3)	0.097(5)
Δ_K/kHz	4.93(5)	0.290(8)
δ_J/kHz	-0.0004(2)	0.0055(6)
δ_K/kHz	-0.26(2)	0.48(2)
κ^a	-0.91	-0.78
F_0^b/GHz	160.8(6)	160.5(9)
δ/rad	0.549(4)	0.905(2)
ε/rad	3.03(5)	2.472(4)
V_3/kJ mol^{-1}	4.60(2)	4.54(3)
N^c	42	47
N_T^d	57	78
σ^e/kHz	1.8	2.5

[a] Asymmetry parameter, $\kappa = (2B - A - C)/(A - C)$. [b] See text for description of the internal rotation constants: F_0, δ, ε, and V_3. [c] Number of rotational transitions included in fit. [d] Total number of A and E symmetry components included in fit. [e] Root-mean-square deviation of residuals.

Compared to MBF, MM contains two additional rotatable bonds, resulting in a richer conformational landscape. Five conformers of MM were located, as illustrated in Fig. 3. In all but the highest energy conformer, MM-V, the methyl group is oriented in the *Z* conformation. The two lowest energy conformers contain an intramolecular hydrogen bond. In the global minimum, MM-I, the hydrogen bond involves the carbonyl oxygen atom (OH···O=C), forming a nearly planar five-membered ring. In MM-II, the ester group is rotated such that the intramolecular hydrogen bond involves the sp^3 oxygen atom (OH···O–C), rather than the sp^2 oxygen atom of the carbonyl group; in this case, the five-membered ring is no longer nearly planar. In MM-III and MM-IV, the intramolecular hydrogen bond is broken because the hydroxyl group is rotated away from the ester group; otherwise, the structures are analogous to MM-I and MM-II. The calculated rotational constants and dipole moments are listed in Table 3.

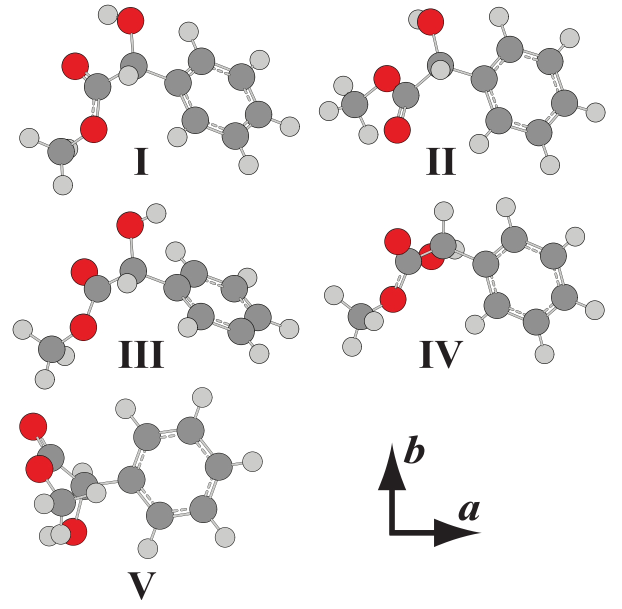

Fig. 3 Conformers of methyl mandelate, optimized at the B3LYP/6-311++G(d,p) level of theory.

Table 3 Calculated relative energies, abundances, rotational constants, and dipole moments of five conformers of methyl mandelate at the B3LYP/6-311++G(d,p) level of theory

Constant	MM-I	MM-II	MM-III	MM-IV	MM-V
ΔE^{a}/kJ mol^{-1}	0.00	8.85	13.8	15.1	47.1
ΔG^{b}/kJ mol^{-1}	0.00	10.8	15.0	16.3	49.3
P^{c}/%	98.0	1.73	0.36	0.23	<0.01
A/MHz	1570.37	1733.33	1604.30	1691.54	1619.58
B/MHz	637.04	590.52	596.28	575.11	656.81
C/MHz	529.89	527.76	545.89	563.86	603.73
κ^{d}	-0.79	-0.90	-0.90	-0.98	-0.90
$\lvert\mu_a\rvert$/D	0.53	0.57	1.72	1.65	2.11
$\lvert\mu_b\rvert$/D	3.04	0.10	2.33	1.20	2.66
$\lvert\mu_c\rvert$/D	0.33	2.43	1.32	0.55	0.34

[a] Total energy (sum of electronic and zero-point energies) relative to minimum energy conformer. [b] Relative free energy. [c] Percent abundance at 323 K, the source temperature, based on relative free energy. [d] Asymmetry parameter, $\kappa = (2B - A - C)/(A - C)$.

Based on the relative free energies calculated at the B3LYP/6-311++G(d,p) level (see Table 3), the abundance of MM-I is predicted to be about 98%, so this is the conformer we targeted in our spectral search. A representative transition, exhibiting methyl internal rotation splitting similar to that of MBF, is shown in Fig. 2. The rotational, centrifugal distortion, and internal rotation constants resulting from the spectroscopic analysis are listed in Table 2. As shown in Table S2, 47 transitions, all *b*-type, were measured. On average, the calculated rotational constants of MBF-I are about 1% lower than those determined experimentally. This discrepancy is slightly larger in magnitude than that obtained for MBF. The asymmetry parameter, κ, based on the experimental rotational constants (-0.78) is consistent with only MM-I (κ = -0.79 from the calculated rotational constants). In addition, only MM-I features a *b*-type dipole moment component that is much larger than the *a*- and *c*-type dipole moment components, consistent with the fact that only *b*-type transitions were detected. We assign the experimental spectrum to MM-I. This is the same conformer identified by Le Barbu-Debus et al., using IR/UV double-resonance spectroscopy.[18] No additional, unassigned lines were observed, consistent with the low predicted abundance of the next most stable conformer, MM-II, less than 2%. In contrast, for solutions of MM in *n*-hexane, Tsui et al. report having observed distinctive OH stretching vibrational bands for both MM-I and MM-II.[17]

We note that the dihedral angle of the carbon "backbone", which dictates the relative orientation of the bulky phenyl and ester groups, changes significantly upon reduction, from 5.8° in MBF I to 91.6° in MM I. In the laboratory, homo- and heterogeneous enantioselective reduction is done in solution – for example, using methanol as a solvent.[15] Such a protic solvent may, for example, form hydrogen-bonded complexes with the reactant and product molecules and consequently alter the structures and the related conformational distribution of the solutes from the gas phase ones. In the previous vibrational circular dichroism and IR study of MM in methanol and chloroform, it was showed that the dominant conformer of MM at room temperature in solution largely retains the same gas phase carbon "backbone" geometry even with the insertion of one or two methanol molecules into the intramolecular hydrogen bond (OH···O=C) and with the inclusion of bulk solvent environment.[21] While no corresponding study has been reported for MBF, for the sake of discussion, we tentatively assume that the aforementioned dihedral angles remain approximately the same for both MBF and MM in methanol solution as in the gas phase. If we also assume that a given catalyst first binds to MBF in its lowest energy conformation and, after reaction, releases MM in its lowest energy conformation, our results imply that the catalyst must be able to accommodate a dramatic alteration in the structure of the substrate to be efficient. Furthermore, the enhanced enantioselectivity of nano-confined catalysts for the reduction of MBF may be attributed in part to these structural changes;[15] it is conceivable that, for a given binding scenario, there may be room for the ester group to rotate to one side of the aromatic ring and not the other. Future microwave spectroscopic studies of step-wise addition of solvent molecules to MBF and MM would provide further insight in this regard.

Hydrogen bonding

QTAIM is a powerful and popular method for the characterization of intra-[48,49] and intermolecular[50,51] hydrogen bonding. Since the two lowest energy conformers of MM contain an intramolecular hydrogen bond, we present a discussion of their QTAIM properties. In the paradigm of QTAIM,[40,41] molecules are partitioned into quantum atoms that are separated by interatomic surfaces; these, in turn, are characterized at any point by zero flux of the electron density gradient, $\nabla\rho$. Atomic properties, such as the electron population, can be determined by integrating over the volume of the resulting atoms or "basins". Of course, summation of a certain atomic property over all atoms must give the molecular property. Furthermore, any point at which $\nabla\rho=0$ is a critical point in the topology of the molecule. Critical points that are maxima (attractors of electron density) in all dimensions coincide with nuclei, and critical points that are maxima in all but one dimension (the bond path) are bond critical points (BCPs). Below, we investigate hydrogen bonding using local BCP properties and integrated atomic properties. The B3LYP calculations discussed above are used as the basis of our QTAIM analysis of hydrogen bonding, because (i) the predicted structures of the assigned conformers closely match the experimental structures and (ii) the electron densities predicted using the B3LYP functional are reasonable approximations to those from more computationally expensive post-Hartree–Fock wavefunction-based methods.[52]

The type and strength of interactions involved in a given bonding scenario are reflected by the local properties of the BCP along the corresponding bond path. The electron density and the Laplacian, $\nabla^2\rho$ (the curvature of the electron density) at the H···O BCPs (see Fig. S1) are particularly illustrative. As shown in Table 4, the electron densities and Laplacians for both conformers are in the typical range of hydrogen bonds: 0.002-0.034 and 0.024-0.139 au, respectively.[53] The electron density of the H···O BCP of MM-I (0.024 au) is greater than that of MM-II (0.019 au). That is, the BCP of MM-I is a stronger attractor of electron density than that of MM-II; in other words, the OH···O=C hydrogen bond is stronger than the OH···O–C hydrogen bond. Consequently, the electronic potential energy density, $V(r)$, of the H···O BCP of MM-I (-0.020 au) is greater in magnitude than that of MM-II (-0.016 au). The Laplacians are positive, indicating that the electron density at the BCP is locally depleted – a signature of non-covalent, closed shell interactions.[40] In order to investigate the effect of hydrogen bonding on atomic properties, we compare MM-I and MM-II to their analogues without an intramolecular hydrogen bond: MM-III and MM-IV, respectively. Upon formation of both types of hydrogen bond, the volume and electronic population of the hydrogen atom of the hydroxyl group decrease, but the energy increases (see Table 4); all three changes meet the general criteria of hydrogen bonding.[53]

Table 4 Local bond critical point properties and integrated atomic properties related to hydrogen bonding in methyl benzoylformate and methyl mandelate, calculated at the B3LYP/6-311++G(d,p) level of theory

Constant	MBF-I	MM-I	MM-II
Bonding	CH···O=C	OH···O=C	OH···O–C
r(H···O)/Å	2.51	2.06	2.16
ρ[a]/au	0.011	0.024	0.019
$\nabla^2\rho$/au	0.041	0.10	0.088
$V(r)$/au	-0.0066	-0.020	-0.016
ΔN(H)[b]/au	-0.020	-0.026	-0.019
Δv(H)/au	-4.8	-4.9	-3.6
ΔE(H)/au	0.0036	0.017	0.0082
$E_{HB}[V(r)]$[c]/kJ mol^{-1}	8.70	26.1	20.9
$E_{HB}(\rho)$[d]/kJ mol^{-1}	–	11.0	5.82

[a] Local BCP properties: electron density, ρ; Laplacian, $\nabla^2\rho$; and electronic potential energy density, $V(r)$. [b] Integrated atomic properties: changes in electronic population, ΔN(H), atomic volume, Δv(H), and atomic energy, ΔE(H), of the hydrogen atom upon formation of hydrogen bond. [c] Hydrogen bond energy calculated from the electronic potential energy density, $V(r)$, at the bond critical point (based on Ref. 54). [d] Hydrogen bond energy calculated from the electron density, ρ, at the bond critical point (based on Ref. 59). No parameterization is available for CH···O=C bonding.

QTAIM can also be used to estimate hydrogen bond energy, E_{HB}. For example, the hydrogen bond energy has been shown to be proportional to $V(r)$ at the corresponding BCP, according to the equation $E_{HB}=-0.5a_0^3V(r)$, where a_0 is the Bohr radius.[54-55] Based on the values of $V(r)$ for the H···O BCPs in MM-I and MM-II, the hydrogen bond energies are estimated to be 26.1 and 20.9 kJ mol^{-1}, respectively. The H···O bond lengths in MM-I and MM-II (2.06 and 2.16 Å, respectively) are in the range of moderate hydrogen bonds, which typically have hydrogen bond energies from about 16 to 60 kJ mol^{-1} – since the interactions involved, though principally electrostatic, are partly covalent.[56] From this perspective alone, the estimates of hydrogen bond energies based on $V(r)$ are reasonable. However, the hydrogen bond energy can also be estimated from the magnitude of the redshift of the OH stretching vibration, $\Delta\nu_{OH}$, according to the empirical relationship $E_{HB}=1.38(\Delta\nu_{OH}-40)^{1/2}$, where $\Delta\nu_{OH}$ is in wavenumber.[57] For the OH···O=C hydrogen bond, Tsui et al.[17] observed a redshift of -93 cm^{-1}, allowing us to estimate a hydrogen bond energy of 10.1 kJ mol^{-1}. This value is significantly lower than the above energies based on $V(r)$, suggesting that they are over-estimated – as observed in a recent study.[58] Furthermore, this conclusion is consistent with the total energies of the conformers with and without hydrogen bonding. First, MM-I is only 14.3 kJ mol^{-1} lower in energy than MM-III, its analogue without an intramolecular hydrogen bond; similarly, MM-II is 6.9 kJ mol^{-1} lower in energy than MM-IV. Consequently, we turn to a recently devised semi-empirical relationship between hydrogen bond energy and electron density at the BCP, ρ_{BCP}: $E_{HB}=-3.09+239\rho_{BCP}$.[59] The resulting estimates of bond energies for MM-I and MM-II (11.0 and 5.8 kJ mol^{-1}, respectively) are more reasonable in the above context.

In passing, we note that weak CH···O=C hydrogen bonds were identified in MM-II and MBF-I (see Fig. S1). For instance, in MBF-I, a BCP is located between the carbonyl oxygen atom of the ester group and the nearest hydrogen atom of the ring, forming a six-membered ring, with all of the atoms – except the carbonyl oxygen atom – in a plane. The electron density is 0.011 au, and the Laplacian is 0.041 au; because the electron density is much lower for this bond than the conventional hydrogen bonds discussed above, it is much weaker. Based on a comparison of integrated atomic properties of the H···O hydrogen atom and a non-bonded reference, the hydrogen atom at the *para* position of the ring, further QTAIM criteria for hydrogen bonding are met.[53] For example, the H···O hydrogen atom has less charge and volume, but more energy, than the reference hydrogen atom (see Table 4).

Internal dynamics

The spectroscopic fits performed using the program XIAM resulted in internal rotation constants (see Table 2), in addition to the rotational and centrifugal distortion constants discussed above. The following four internal rotation constants were fitted: F_0, the methyl top rotation constant, which is inversely proportional to the moment of inertia of the methyl top about its axis; δ, the angle between the methyl top axis and the *a* principal inertial axis; ε, the angle between the *b* principal axis and the projection of the methyl top axis onto the *bc* plane; and V_3, the barrier height. At the outset, we note that the experimental values of angles ε and δ are consistent with the conformational structures we assigned to our spectra above. For MBF, δ and ε are found to be 0.549(4) and 3.03(5) rad, respectively, in close agreement with the values of 0.53 and 3.09 rad calculated for MBF-I. Similarly, for MM, δ and ε are found to be 0.905(2) and 2.472(4) rad, respectively, in fairly good agreement with the values of 0.81 and 2.35 rad calculated for MM-I.

The experimental barrier heights for MBF and MM are 4.60(2) and 4.54(3), respectively. Theoretical barrier heights were calculated by locating the transition states of methyl internal rotation, in which a given hydrogen atom of the methyl top is eclipsed by the carbonyl oxygen atom of the ester group. The calculated barriers were *ZPE*-corrected for the minima and the transition states. At the B3LYP/6-311++G(d,p) level of theory, the barrier heights for MBF-I and MM-I are 2.39 and 2.57 kJ mol^{-1}, respectively. Besides being more than 40% lower than the experimental values, these calculated values do not predict the correct relative magnitude of the barriers. Consequently, we chose to run higher-level second-order Møller-Plesset (MP2) perturbation theory[60] calculations, with the 6-311++G(d,p) basis set. The resulting values for MBF-I and MM-I are 4.58 and 4.52 kJ mol^{-1}, respectively, in very good agreement with the experimental values (less than 0.5% discrepancy). Similarly, MP2 calculations were shown to accurately predict the barrier height for methyl lactate.[30]

Table 5 Changes in bond lengths, local bond critical point densities, and integrated electronic populations and atomic energies related to internal rotation in *cis*-methyl formate, methyl benzoylformate, and methyl mandelate, calculated at the MP2/6-311++G(d,p) level of theory

Constant	*cis*-MF	MBF-I	MM-I
V_3^{MP2}/kJ mol^{-1}	4.87	4.58	4.52
$r[\mathrm{C{=}O\cdots H(CH_2)}]_{\mathrm{MIN}}{}^{a}$/Å	2.646	2.647	2.644
$r[\mathrm{C{=}O\cdots H(CH_2)}]_{\mathrm{TS}}{}^{b}$/Å	2.278	2.286	2.276
Δr(H1–C2)^{c}/Å	-0.0020	-0.0017	-0.0018
Δr(C2–O3)/Å	0.0014	0.0019	0.0016
Δr(O3–C4)/Å	0.0029	0.0024	0.0014
Δr(C4=O5)/Å	-0.0010	-0.0011	-0.0008
$\Delta\rho$(H1–C2)/au	0.0024	0.0020	0.0022
$\Delta\rho$(C2–O3)/au	-0.0019	-0.0022	-0.0022
$\Delta\rho$(O3–C4)/au	-0.0036	-0.0034	-0.0029
$\Delta\rho$(C4=O5)/au	0.0007	0.0008	0.0006
ΔN(H1)/au	-0.0276	-0.0289	-0.0290
$\Delta N[\mathrm{C2(H_2)}]$/au	0.0292	0.0278	0.0274
ΔN(O3)/au	-0.0020	0.0002	0.0009
ΔN(C4)/au	-0.0057	-0.0005	-0.0032
ΔN(O5)/au	0.0064	0.0013	0.0035
ΔN(R)/au	-0.0006	0.0000	-0.0003
ΔE(H1)/au	0.0093	0.0089	0.0094
$\Delta E[\mathrm{C2(H_2)}]$/au	-0.0127	-0.0108	-0.0109
ΔE(O3)/au	0.0091	0.0072	0.0051
ΔE(C4)/au	0.0105	0.0025	0.0073
ΔE(O5)/au	-0.0135	-0.0034	-0.0075
ΔE(R)/au	-0.0003	-0.0024	-0.0014

[a] The average distance (in the minimum energy structure) between the carbonyl oxygen atom of the ester group and the gauche hydrogen atoms of the methyl top. [b] The distance (in the transition state structure) between the carbonyl oxygen atom of the ester group and the eclipsed hydrogen atom of the methyl top. [c] Changes in properties incurred in going from minimum to transition state.

The experimental ester methyl barrier heights are considerably lower than that of methyl formate (4.98 kJ mol^{-1}),[61] and only slightly higher than that of methyl fluoroformate (4.51 kJ mol^{-1}).[62] In the past, differences in barrier heights of ester methyl groups have been attributed to differences in the distance between the eclipsed hydrogen atom and the carbonyl oxygen atom in the transition state.[62] For comparison, we performed geometry optimization and frequency analysis calculations for the minimum and transition state of *cis*-methyl formate (*cis*-MF) at the MP2/6-311++G(d,p) level of theory. In the minimum energy structures of *cis*-MF, MBF-I, and MM-I, the average distances between the carbonyl oxygen atom of the ester group and the gauche hydrogen atoms of the methyl top are 2.646, 2.647, and 2.644 Å, respectively; in the transition state structures, the distances between the carbonyl oxygen atom and the eclipsed hydrogen atom are 2.278, 2.286, and 2.276 Å, respectively (see Table 5). Since these distances do not correlate with the barrier heights based on the same calculated structures, proximity alone cannot explain the experimental trend in the barrier heights.

A QTAIM analysis can provide insight into the underlying chemistry causing barriers to internal rotation;[63-65] for example, the specific atoms destabilized in the transition state can be identified.[66] Since our MP2 calculations gave much more accurate barrier heights than the B3LYP calculations, we use them as the basis for our discussion below. (The keywords "density=current" and "output=wfx" were used to export a given MP2 wavefunction to an input file for analysis in Multiwfn.) In Table 5, we summarize changes in bond lengths, electron densities, atomic electronic populations, and atomic energies that occur in going from the minimum to the transition state.

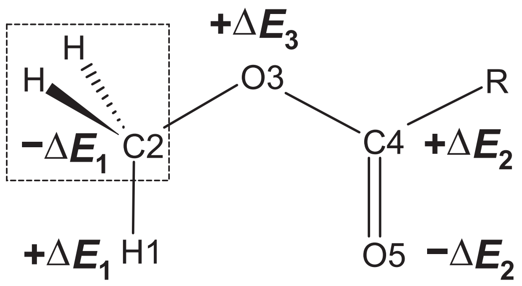

Fig. 4 Simplified illustration of the atoms stabilized and destabilized by methyl internal rotation. The dotted square indicates the methylene bridge, which is treated as one unit in the current discussion. + (or –) ΔE_i indicates the approximate energy of destabilization (or stabilization) associated with the respective atoms in the figure. See text for a detailed description.

To begin, we note that internal rotation has comparatively little effect on the sum of electronic populations or energies of the atoms outside of the methyl ester group. We denote all these outside atoms as R in Fig. 4. In going from the staggered to eclipsed positions, the hydrogen atom (H1 in Fig. 4) loses electronic population to the other three atoms of the methyl group. As a result of this shift in electron density, H1 is significantly destabilized (for example, 0.0094 au in MM). On the other hand, the "methylene bridge", $C2(H_2)$, indicated with a dotted square in Fig. 4, is stabilized to approximately the same extent (-0.0109 au in MM). Similarly, C4 is destabilized by a loss of electronic population to O5, which is stabilized to roughly the same extent. For the related H1–C2 and C4=O5 bonds, electron densities at their BCPs increase, and their bond lengths decrease. In contrast, for the C2–O3 and O3–C4 bonds, electron densities at the BCPs decrease. The resulting increase in bond lengths coincides with a decrease in both repulsive and attractive forces between O3 and its bonding partners, C2 and C4. Since O3 is destabilized in the transition state, the decrease in attractive forces dominates. Since there is no compensation for the destabilization of O3 as there is in the cases of H1 and C4, the total energy of the transition state is greater than that of the minimum. Consequently, for the three esters considered here, the trend in barrier height agrees with the trend in destabilization of O3: $\Delta E(O3)_{MM} < \Delta E(O3)_{MBF} < \Delta E(O3)_{MF}$. The internal rotation barrier heights for the R-C(=O)-O-CH_3 type ester methyl tops have previously been found to obey an empirical inverse relationship with the electron attracting capability of the R group.[30,62] The previous rationale was that the higher electron attracting substituent R strengthens the C–O and C=O bonds, therefore causing an increase in the $r[C{=}O\cdots H(CH_2)]$ distance. This rationale does not seem adequate in the context of the current analysis. Rather, the current analysis emphasizes the importance of examining both the minimum and transition states in order to rationalize the changes in barrier heights, which can be related to $\Delta E(O3)$, the destabilization of the oxygen atom that links the carbonyl and methyl groups.

Conclusions

In summary, we have made the first measurements of the rotational spectra of MBF and MM, species that are representative of a prochiral reactant and chiral product of enantioselective reduction, respectively. We have also investigated intramolecular hydrogen bonding using QTAIM and determined the barriers to methyl internal rotation using the splittings in the observed transitions. We propose that the internal rotation barrier height depends on the degree of destabilization of the sp^3 oxygen atom of the ester group. Based on the minimum energy conformers of MBF and MM observed, we have tracked the structural changes in the gas phase – highlighted by a 90° change in the dihedral angle of the carbon "backbone" – that likely indicate that similarly significant changes occur upon reduction of MBF in solution. The thorough understanding of structural changes provided by our findings, if complemented by future studies of step-wise solvation of MBF and MM, could aid in the design of future catalysts with improved efficiency and enantioselectivity.

Acknowledgements

This research was funded by the Natural Sciences and Engineering Research Council of Canada (NSERC). Computing resources were provided by Westgrid and Compute/Calcul Canada. EGS thanks NSERC for a Postgraduate Scholarship, and the University of Alberta for a President's Doctoral Prize of Distinction. YX holds a Tier I Canada Research Chair (CRC) in Chirality and Chirality Recognition and WJ holds a CRC in Cluster Science.

References

1 V. S. Lamzin, Z. Dauter and K. S. Wilson, *Curr. Opin. Struct. Biol.*, 1995, **5**, 830.
2 S.-J. Lin and L. Guarente, *Curr. Opin. Struct. Biol.*, 2003, **15**, 241.
3 A. I. Meyers and J. D. Brown, *J. Am. Chem. Soc.*, 1987, **109**, 3155.
4 J.-L. Vasse, V. Levacher, J. Bourguignon and G. Dupas, *Tetrahedron*, 2003, **59**, 4911.
5 X.-Q. Fang, Y.-C. Liu, G.-W. Wang and Y.-P. Ke, *Res. Chem. Intermed.*, 2006, **32**, 603.
6 V. A. Burgess, S. G. Davies and R. T. Skerlj, *Tetrahedron Asymmetry*, 1991, **2**, 299.
7 P. Binay, G. Dupas, J. Bourguignon and G. Queguiner, *Tetrahedron Lett.*, 1988, **29**, 931.
8 K. Skog and O. Wennerström, *Tetrahedron Lett.*, 1992, **33**, 1751.
9 X. Li and D. D. Tanner, *Tetrahedron Lett.*, 1996, **37**, 3275.
10 N. Kanomata and T. Nakata, *Angew. Chem. Int. Ed.*, 1997, **36**, 1207.
11 U. Gran, *Tetrahedron*, 2003, **59**, 4303.
12 J. Zhao, N.-X. Wang, W.-W. Wang, G.-X. Wang, Y.-H. Liu, L. Li, J.-L. Yu and X.-L. Tang, *Molecules*, 2007, **12**, 979.
13 N.-X. Wang and J. Zhao, *Adv. Synth. Catal.*, 2009, **351**, 3045.

14 N. Maeda, S. Sano, T. Mallat, K. Hungerbühler and A. Baiker, *J. Phys. Chem. C*, 2012, **116**, 4182.
15 J. M. Thomas and R. Raja, *Accounts Chem. Res.*, 2008, **41**, 708.
16 I. Suryanarayana, B. Subrahmanyam and N. V. Subba Rao, *Proc. Indian Acad. Sci.*, 1975, **82**, 55.
17 H.-W. Tsui, N.-H. L. Wang and E. I. Franses, *J. Phys. Chem. B*, 2013, **117**, 9203.
18 K. Le Barbu-Debus, M. Broquier, A. Mahjoub and A. Zehnacker-Rentien, *J. Phys. Chem. A*, 2008, **112**, 9731.
19 M. Albrecht, A. Borba, K. Le Barbu-Debus, B. Dittrich, R. Fausto, S. Grimme, A. Mahjoub, M. Nedić, U. Schmitt, L. Schrader, M. A. Suhm, A. Zehnacker-Rentien and J. Zischang, *New J. Chem.*, 2010, **34**, 1266.
20 M. Nedić and M. A. Suhm, *Cryst. Growth Des.*, 2012, **12**, 1933.
21 M. R. Poopari, Z. Dezhahang and Y. Xu, *Phys. Chem. Chem. Phys.*, 2013, **15**, 1655.
22 J.-H. Shi, Z.-J. Ding and Y. Hu, *J. Mol. Model.*, 2012, **18**, 803.
23 K. Ogata, H. Odashima, K. Takagi and S. Tsunekawa, *J. Mol. Spectrosc.*, 2004, **225**, 14.
24 F. Willaert, H. Møllendal, E. Alekseev, M. Carvajal, I. Kleiner and J. Demaison, *J. Mol. Struct.*, 2006, **795**, 4.
25 V. Ilyushin, A. Kryvda and E. Alekseev, *J. Mol. Spectrosc.*, 2009, **255**, 32.
26 B. Tercero, L. Margulès, M. Carvajal, R. A. Motiyenko, T. R. Huet, E. A. Alekseev, I. Kleiner, J. C. Guillemin, H. Møllendal and J. Cernicharo, *Astron. Astrophys.*, 2012, **538**, A119.
27 J. L. Neill, M. T. Muckle, D. P. Zaleski, A. L. Steber, B. H. Pate, V. Lattanzi, S. Spezzano, M. C. McCarthy and A. J. Remijan, *Astrophys. J.*, 2012, **755**, 153.
28 S. Melandri, B. M. Giuliano, A. Maris, L. B. Favero, P. Ottaviani, B. Velino and W. Caminati, *J. Phys. Chem. A*, 2007, **111**, 9076.
29 P. Ottaviani, B. Velino and W. Caminati, *Chem. Phys. Lett.*, 2006, **428**, 236.
30 N. Borho and Y. Xu, *Phys. Chem. Chem. Phys.*, 2007, **9**, 1324.
31 J. Thomas, J. Yiu, J. Rebling, W. Jäger and Y. Xu, *J. Phys. Chem. A*, 2013, **117**, 13249.
32 E. G. Schnitzler and W. Jäger, *Phys. Chem. Chem. Phys.*, 2014, **16**, 2305.
33 E. G. Schnitzler, B. L. M. Zenchyzen and W. Jäger, *Astrophys. J.*, 2015, **805**, 141.
34 Y. Xu and W. Jäger, *J. Chem. Phys.*, 1997, **106**, 7968.
35 V. N. Markov, Y. Xu and W. Jäger, *Rev. Sci. Instrum.*, 1998, **69**, 4061.
36 Y. Xu, J. Van Wijngaarden and W. Jäger, *Int. Rev. Phys. Chem.*, 2005, **24**, 301.
37 M. J. Frisch, *et al.*, *Gaussian09*, *Revision D.01*, Gaussian, Inc., Wallingford, CT, 2013.
38 A. D. Becke, *J. Chem. Phys.*, 1993, 98, 5648.
39 R. Ditchfield, W. J. Hehrf and J. A. Pople, *J. Chem. Phys.*, 1971, **54**, 724.
40 R. F. W. Bader, *Atoms in Molecules: A Quantum Theory*, Oxford University Press, New York, 1990.
41 R. F. W. Bader, *Chem. Rev.*, 1991, **91**, 893.
42 T. Lu and F. Chen, *J. Comput. Chem.*, 2012, **33**, 580.
43 C. F. Matta and R. J. Boyd, in *The Quantum Theory of Atoms in Molecules: From Solid State to DNA and Drug Design*, ed. C. F. Matta and R. J. Boyd, Wiley, New York, 2007, pp. 29-30.
44 C. M. Western, *PGOPHER*, *A Program for Simulating Rotational Structure*, University of Bristol, http://pgopher.chm.bris.ac.uk.
45 H. Hartwig and H. Dreizler, *Z. Naturforsch.*, 1996, **51A**, 923.
46 J. K. G. Watson, *J. Chem. Phys.*, 1967, **46**, 1935.
47 D. M. Pawar, A. A. Khalil, D. R. Hooks, K. Collins, T. Elliott, J. Stafford, L. Smith and E. A. Noe, *J. Am. Chem. Soc.*, 1998, **120**, 2108.
48 P. L. A. Popelier and R. F. W. Bader, *Chem. Phys. Lett.*, 1992, **189**, 542.
49 M. Petković and M. Etinski, *RSC Adv.*, 2014, **4**, 38517.
50 J. R. Cheeseman, M. T. Carroll and R. F. W. Bader, *Chem. Phys. Lett.*, 1998, **143**, 450.
51 O. O. Brovarets, R. O. Zhurakivsky and D. M. Hovorun, *J. Comput. Chem.*, 2014, **35**, 451.
52 P. Popelier, *Atoms in Molecules: An Introduction*, Prentice Hall, Harlow, 2000, p. 11.
53 U. Koch and P. L. A. Popelier, *J. Phys. Chem.*, 1995, **99**, 9747.
54 E. Espinosa, E. Molins and C. Lecomte, *Chem. Phys. Lett.*, 1998, **285**, 170.
55 I. Mata, I. Alkorta, E. Espinosa and E. Molins, *Chem. Phys. Lett.*, 2011, **507**, 185.
56 G. A. Jeffrey, *An Introduction to Hydrogen Bonding*, Oxford University Press, New York, 1997, pp. 12-16.
57 A. V. Iogansen, *Spectrochim. Acta Part A*, 1999, **55**, 1585.
58 A. V. Vashchenko and A. V. Afonin, *J. Struct. Chem.*, 2014, **55**, 636.
59 T. Yu. Nikolaienko, L. A. Bulavin and D. M. Hovorun, *Phys. Chem. Chem. Phys.*, 2012, **14**, 7441.
60 C. Møller and M. S. Plesset, *Phys. Rev.*, 1934, **46**, 618.
61 R. F. Curl, *J. Chem. Phys.*, 1959, **30**, 1529.
62 G. Williams, N. L. Owens and J. Sheridan, *Trans. Faraday Soc.*, 1971, **67**, 922.
63 R. F. W. Bader, J. R. Cheeseman, K. E. Laidig, K. B. Wiberg and C. Breneman, *J. Am. Chem. Soc.*, 1990, **112**, 6530.
64 A. M. Graña and R. A. Mosquera, *J. Mol. Struct.*, 2000, **556**, 69.
65 J. A. Platts and M. P. Coogan, *J. Chem. Soc. Perkin Trans.*, 2000, 1075.
66 C. M. Breneman and J. A. Moore, *Struct. Chem.*, 1997, **8**, 13.